JACS
JOURNAL OF THE AMERICAN CHEMICAL SOCIETY

Communication

pubs.acs.org/JACS

Metallic Nanocages: Synthesis of Bimetallic Pt–Pd Hollow Nanoparticles with Dendritic Shells by Selective Chemical Etching

Liang Wang[†,‡] and Yusuke Yamauchi*[,†,§]

[†]World Premier International Research Center for Materials Nanoarchitectonics, National Institute for Materials Science, Namiki 1-1, Tsukuba, Ibaraki 305-0044, Japan

[‡]State Key Laboratory of Electroanalytical Chemistry, Changchun Institute of Applied Chemistry, Chinese Academy of Sciences, Changchun, Jilin 130022, China

[§]Faculty of Science and Engineering, Waseda University, 3-4-1 Ohkubo, Shinjuku, Tokyo 169-8555, Japan

Supporting Information

ABSTRACT: We report a facile synthesis of Pt–Pd bimetallic nanoparticles, named "metallic nanocages", with a hollow interior and porous dendritic shell. This synthesis is easily achieved by selective chemical etching of Pd cores from dendritic Pt-on-Pd nanoparticles. The obtained Pt–Pd nanocages show superior catalytic activity for methanol oxidation reaction compared to other Pt-based materials reported previously.

Currently, synthesis and application of hollow inorganic nanoparticles with interior cavities and controlled shell architectures are attracting considerable interest.[1] In general, hollow nanoparticles can be fabricated by a templating approach, the Kirkendall effect, galvanic replacement, and so on. In comparison with their solid counterparts, hollow nanoparticles have a higher surface area and lower density, which are highly desirable structural features for various applications, such as catalysis, energy storage/conversion, sensing, controlled delivery, etc.

Among various hollow nanoparticles, metallic hollow nanoparticles are of great importance due to their excellent catalytic property. Specifically, the platinum hollow nanoparticle with a highly accessible surface area represents a promising catalyst.[2] The hollow architecture highly favors desirable high mass activity of very rare and expensive Pt catalysts. For instance, Pt hollow nanoparticles show a larger surface area and enhanced electrocatalytic performance in methanol oxidation reaction (MOR) in comparison with solid Pt nanoparticles.[3] The electrocatalytic activity of hollow Pt nanoparticles can be further enhanced by tailoring their shapes, sizes, and compositions. Much effort has been devoted to the creation of hollow nanoparticles toward promising Pt catalysts with enhanced catalytic performance and improved Pt utilization efficiency. Accordingly, various Pt-based hollow nanoparticles with different shapes and compositions have been demonstrated, such as Pt–Co, Pt–Ni, Pt–Ag, Pt–Pd, and so on.[4]

It is noted that the previously reported Pt-based hollow nanoparticles have compact and smooth exteriors. Therefore, guest molecules cannot access the internal surface. In most cases, the inner surface has not been effectively utilized, although the inner surface can be used as a highly catalytic site in catalytic reaction. It is expected that the creation of a nanoporous shell allows for effective use of the inner surface in hollow nanoparticles, thereby favoring great improvement of the accessible surface area. In comparison with exterior catalytic sites, the interior catalytic sites are not susceptible to particle agglomeration in the catalytic reaction. Thus, exquisite nanoarchitecture in the shell is highly favorable for the further enhancement of catalytic activity.

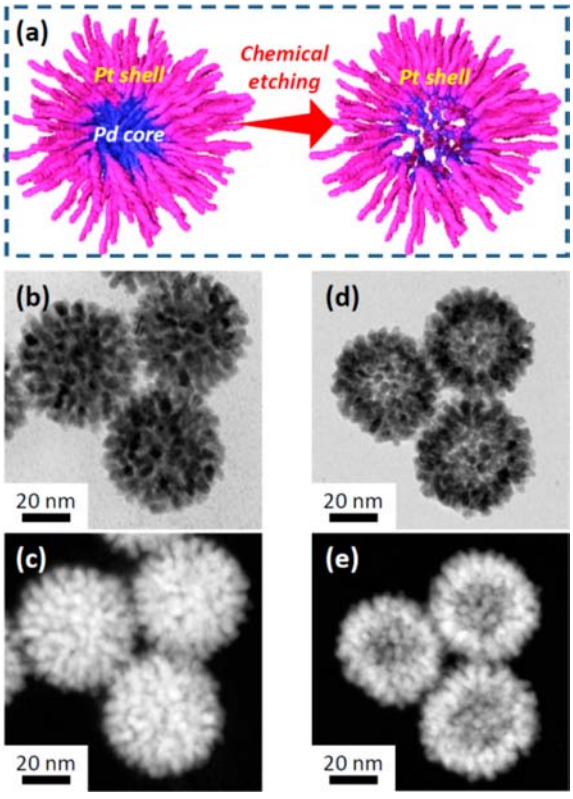

Figure 1. (a) Schematic presentation for formation of bimetallic dendritic nanocage with hollow interior and porous dendritic wall. (b–e) TEM and HAADF-STEM images for (b,c) dendritic Pt-on-Pd nanoparticles before chemical etching and (d,e) dendritic nanocages after chemical etching.

Received: July 28, 2013
Published: October 30, 2013

dx.doi.org/10.1021/ja407773x | J. Am. Chem. Soc. 2013, 135, 16762–16765

Inspired by this idea, here we newly design dendritic Pt-based hollow nanoparticles, "metallic nanocages", via a sophisticated chemical etching approach using Pt-on-Pd bimetallic dendritic nanoparticles as the starting material (Figure 1). The hollow interior and dendritic shell can provide abundant catalytic sites, leading to very high electrocatalytic activity relative to that of the commercially available Pt product.

Dendritic Pt-on-Pd nanoparticles as the starting material were synthesized by a one-step route in an aqueous solution at room temperature with the assistance of block copolymers.[5] In a typical synthesis, an aqueous solution (5.0 mL) containing 0.10 mmol of Na_2PtBr_6, 0.05 mmol of K_2PdBr_4, and Pluronic F127 (0.05 g) was placed in a beaker, and then 0.1 M ascorbic acid (5.0 mL) was quickly added while stirring. The mixture solution was stirred for 8 h at room temperature. By consecutive washing/centrifugation cycles, the residual Pluronic F127 was completely removed. The colloidal suspension was obtained. This approach utilized the temporal separation of the depositions of Pd and Pt, leading to the spontaneous formation of Pt-on-Pd dendritic nanoparticles. During the Pt growth, Pluronic F127 played a structure-directing agent role with its hydrophobic poly(propylene oxide) group adsorbing on the deposited Pt surface, facilitating the dendritic Pt formation.[5b] The developed synthetic route was quite different from the previously reported two-step Pd seed-mediated growth method.[6]

The shape and size of the typically synthesized Pt-on-Pd dendritic nanoparticles were characterized by transmission electron microscopy (TEM; Figures 1b,c and S1a). The images obtained by high-angle annular dark-field scanning transmission electron microscopy (HAADF-STEM) at different magnifications clearly showed that the as-prepared sample had well-dispersed nanoparticles with a completely dendritic shape (Figures 2a and S1a), demonstrating the high-yield formation. The particle sizes ranged narrowly from 35 to 50 nm, with an average diameter of 42 nm. Well-defined dendritic shells consisted of plentiful of interconnected nanowires of about 2 nm in width. These randomly aggregated nanowires created nanoporous structures, as illustrated in Figure 1a. The wide-angle X-ray diffraction (XRD) profile showed a metallic face-centered cubic (fcc) structure (Figure S2a). In contrast to other core/shell systems, there are no significant differences in the lattice constants between Pt and Pd fcc crystals, which will be explained later in this paper. Therefore, we cannot distinguish whether a bimetallic Pt−Pd alloy is formed. To make it clear, the corresponding elemental mapping revealed that Pt and Pd were not uniformly distributed in the particles, indicating the formation of a Pt-on-Pd structure consisting of a Pd core and dendritic Pt exterior (Figure 2b−d). The compositional line profile further confirmed such a Pt-on-Pd structure (Figure 2e). From energy-dispersive X-ray spectroscopy (EDS) measurement and ICP analysis, the composition of the Pt-on-Pd dendritic nanoparticles was calculated to be around $Pt_{67}Pd_{33}$, which agreed with the Pt/Pd atomic ratio in the initial precursor solution. This means that all of the Pt and Pd sources are completely reduced.

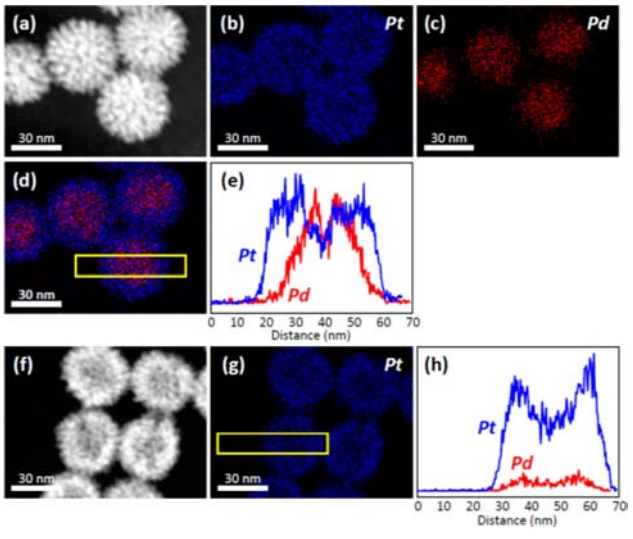

Figure 2. HAADF-STEM images, elemental mapping images and compositional line profiles for (a−e) dendritic Pt-on-Pd nanoparticles before chemical etching and (f−h) dendritic nanocages after chemical etching.

For the preparation of metallic nanocages, selective chemical etching was carried out using the Pt-on-Pd dendritic nanoparticles as the starting material (Figure 1). In a typical synthesis, the Pt-on-Pd dendritic nanoparticles were mixed with an excess amount of concentrated nitric acid, and then the mixture solution was stirred for 5 days at room temperature, allowing selective dissolution of the Pd core. The product was collected by consecutive washing/centrifugation cycles with water.

As illustrated in Figures 1d,e, 2f, and S1b, well-defined dendritic hollow nanoparticles were obtained. The nanocages were strikingly uniform in shape. The average particle size was around 42 nm, which was almost the same size as the starting Pt-on-Pd dendritic nanoparticles before chemical etching. Impressively, the resultant dendritic nanocages had well-developed hollow interiors, which quite differed from the starting sample with solid interiors. The exteriors of the dendritic nanocages were well covered by Pt nanoarms with an average diameter of 2 nm (Figure S1b). The Pt nanoarms were highly branched in various directions, resulting in the porous wall in each individual entity. The porous shells had an average thickness of 14 nm. Nanoscale elemental mapping investigation revealed that Pt was distributed throughout the entire hollow particle (Figure 2g,h). The position of the Pt trace was rich in the exterior region. A small amount of Pd content was also detected even after etching. As revealed by EDS analysis, the Pd was concentrated in the inner surface. The composition was nearly $Pt_{89}Pd_{11}$. The wide-angle XRD profile for dendritic nanocages was for randomly oriented fcc metallic crystals (Figure S2b). It was very difficult to resolve Pt and Pd in the XRD pattern, owing to the fact that the Pt/Pd lattice match ratio was 99.23%.[7]

The selective chemical etching treatment fabricated the dendritic nanocages with hollow interiors and dendritic exteriors with spatially separated nanoarms. These porous characteristics were highly favorable for maximizing the accessible surface area, which was of great importance for achieving high mass activity of a catalyst. The samples before and after chemical etching were characterized by N_2 adsorption/desorption isotherms. Their surface areas were calculated to be 32 and 53 m^2/g, respectively (Figure S3). As seen in the N_2 adsorption isotherms, we could not confirm a clear capillary condensation step which have been typically observed in ordered mesoporous materials.[8] Actually, their pore size distribution curves calculated by the Barrett−Joyner−Halenda (BJH) method showed very random and wide distributions ranging from 2 to 8 nm. TEM data also support the formation of dendritic structures (Figure 1b−e). Therefore, our case is not an ordered mesoporous system, but a dendritic porous system with random pore size distribution.

dx.doi.org/10.1021/ja407773x | J. Am. Chem. Soc. 2013, 135, 16762−16765

Obviously, after chemical etching, the porous structural characteristic greatly improved the surface area in comparison with the starting Pt-on-Pd dendritic nanoparticles. Another important point is that a large hysteresis loop was observed after chemical etching. This appearance is typical for cage-type nanoporous structures, indicating the successful formation of a hollow structure over the entire area. Importantly, the surface area of dendritic nanocages (53 m^2/g) could be compared with the reported highest surface area for unsupported Pt nanowires (53 m^2/g).[9] By way of comparison, previously reported porous Pt nanoparticles and porous Pt nanoballs had surface areas of 14 and 23 m^2/g, respectively.[10]

Interestingly, by reducing the amount of Pt precursor in the initial solution for synthesis of Pt-on-Pd dendritic nanoparticles, the particle size could be effectively reduced, mainly due to the decrease in the Pt shell thickness. With the decrease of the Pt precursor amount to 0.05 mmol, the average particle size was around 28 nm (Figure S4). The compositions were measured to be nearly $Pt_{50}Pd_{50}$, which coincided with the Pt/Pd atomic ratio in the initial precursor solution. This particle size was obviously smaller than that of the typically synthesized Pt-on-Pd dendritic nanoparticles shown in Figures 1b,c, 2a, and S1a.

Such a facile control of Pt and Pd ratios in Pt-on-Pd nanodendrites is highly valuable for their use as starting materials to finely tune the particle sizes and shell thicknesses in the finally obtained nanocages. Even when small-sized Pt-on-Pd nanodendrites (displayed in Figure S4a) were used as the starting material, nanocages with hollow interiors and porous dendritic exteriors were successfully synthesized by a chemical etching treatment (Figure S4b). The obtained composition was $Pt_{81}Pd_{19}$. In comparison with the typically synthesized nanocages (displayed in Figures 1d,e, 2f, and S1b), the ones in Figure S4b had similar porous characteristics (such as hollow interiors and porous dendritic exteriors) and the same size Pt nanoarm, but smaller particle size (~28 nm) and thinner wall thickness (~9 nm). No byproducts, such as irregularly shaped particles, were confirmed, demonstrating high-yield synthesis (Figure S5).

The formation of nanocages is realized by the use of preformed Pt-on-Pd nanodendrites as starting materials followed by selective chemical etching of the Pd cores. Selective etching with concentrated nitric acid solution is based on the difference in chemical stability of the Pd core and Pt exterior. During the chemical etching, the dendritic porous Pt exteriors facilitate the accessibility of etching agents, favoring dissolution of the inner Pd cores. It is noted that use of concentrated nitric acid (14 M) and long etching time (5 days) is necessary for the present etching process. The Pd cores are protected by the Pt shells and have good chemical stability. Other concentrated acid solutions (e.g., sulfuric acid, hydrochloric acid, phosphoric acid) could not dissolve the inner Pd cores at all. Nitric acid solution with lower concentration (e.g., 1 M) was also not effective. The present etching process of the inner Pd cores was extremely slow for 5 days. During the first 4 days, no change of the Pt–Pd nanoparticles could be observed, but in a very limited time within the fifth day, the dissolution of the Pd cores was finished very quickly.

Pd and Pt have the same fcc crystal structures and a very high lattice match (99.23%), and their atoms are highly miscible. At the core/exterior boundary of the Pt-on-Pd nanodendrites, the Pd atoms coherently matched with the lattice structures of the Pt exterior (Figure 4), resulting in the formation of an inserted pseudo Pd–Pt alloy heterointerface.[11] The Pd atoms in the Pd–Pt alloy phase are less vulnerable to chemical etching than the pure Pd core, thereby preserving the Pd–Pt alloyed internal wall even after etching (as illustrated in Figure 1a). In previous works, selective chemical etching has been demonstrated as an efficient method for fabrication of nanostructures with hollow interiors. In most cases, however, the reported porous walls are limited to poorly crystalline and amorphous phases (such as silica and carbon), which are lacking in optical or electrical properties.[12] Different from these materials, highly crystalline shells are generally difficult for etching agents to access the cores. The designed porous dendritic Pt exteriors in the Pt-on-Pd nanodendrites can smartly solve this bottleneck issue and provide porous Pt shells with the desired catalytic property at the same time.

The electrocatalytic performance for MOR was investigated. The obtained nanocages displayed in Figures 1d,e and S4b were denoted as "nanocages I" and "nanocages II", respectively. The original Pt-on-Pd nanodendrites (displayed in Figure 1b,c) and commercially available Pt black (Figure S6) were also tested as reference materials. In the cyclic voltammetry investigation (Figure 3a), two obvious anodic peaks, which were typical MOR

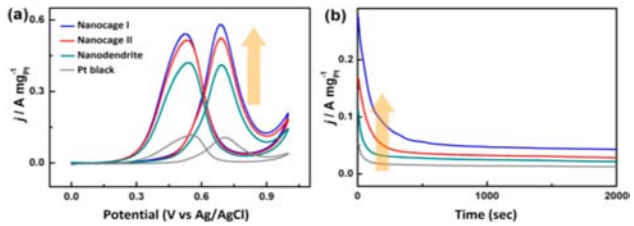

Figure 3. (a) Cyclic voltammograms and (b) chronoamperometric curves for methanol oxidation reaction catalyzed by nanocages I (shown in Figure 1d,e), nanocages II (shown in Figure S4b), nanodendrites (shown in Figure 1b,c), and Pt black (shown in Figure S6) in an aqueous solution containing 0.5 M H_2SO_4 and 1 M methanol. The chronoamperometric curves are recorded at 0.6 V.

features during the positive and negative sweeps, were clearly observed. Our nanocages exhibited better catalytic performance than Pt-on-Pd nanodendrites and Pt black. The mass-normalized current densities were 0.58, 0.52, 0.41, and 0.11 A/mg for nanocages I, nanocages II, nanodendrites, and Pt black, respectively, in the positive direction sweep. The current densities of nanocages I and II were 1.4 and 1.3 times higher, respectively, than those of nanodendrites and 5.3 and 4.7 times higher, respectively, than that of Pt black. Even after normalization of the electrochemical active by the surface areas, the current densities of nanocages I and nanocages II (1.36 and 1.27 $mA{\cdot}mg^2$, respectively) were still higher than nanodendrites and Pt black (1.12 and 0.51 $mA{\cdot}mg^2$, respectively). These results clearly demonstrate that our metallic nanocages show higher catalytic activities than Pt-on-Pd nanodendrites and Pt black in terms of both mass specific activity and surface specific activity. It was further noted that the catalytic performance of nanocages I was also much higher than that of recent state-of-the-art Pt-based nanocatalysts, such as PtRu nanoparticles supported on carbon nanotubes (PtRu/CNTs), Pt nanowires supported on Sn@CNTs nanocable (PtNW-Sn@CNTs), and commercially available PtRu black.[13]

As can be seen in Figure 4, the shells of hollow particles were highly crystallized, and then abundant atomic steps were successfully exposed on the Pt branch surface (as indicated by arrows in Figure 4). Such a unique atomic structure can act as highly active sites for MOR.[14] In chronoamperometric

dx.doi.org/10.1021/ja407773x | J. Am. Chem. Soc. 2013, 135, 16762–16765

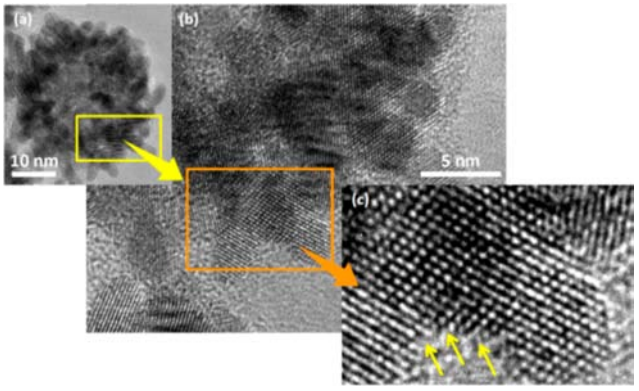

Figure 4. High-resolution TEM images of dendritic nanocages prepared with low-concentrated Pt solution. The atomic steps exposed on the concave surface are indicated by arrows.

investigation recorded at 0.6 V for 2000 s, our nanocages exhibited higher mass current densities than nanodendrites and Pt black during the entire testing time (Figure 3b). Our nanocages with spatially and locally separated Pt nanoarms favored the drastic suppression of the activity loss derived from the undesirable agglomeration of Pt active sites. Considering their hollow and porous dendritic structural features, the enhanced catalytic activities of Pt–Pd nanocages are ascribed to their sufficient accessible active sites at both interior and exterior surfaces. As mentioned above, the atoms of Pd and Pt are highly miscible, and pseudo Pd–Pt alloy phases are formed at the internal surface of the hollow structures, which is favorable for reducing the electronic binding energy in Pt and facilitating the C–H cleavage reaction in methanol decomposition.[11,15]

In summary, we demonstrate a simple and efficient strategy for synthesis of dendritic Pt–Pd nanocages with hollow interiors and porous dendritic shells through selective chemical etching of Pd cores from the preformed Pt-on-Pd nanodendrites. Because they have sufficient catalytic active sites at both their interior and exterior surfaces, our nanocages are highly active catalysts for MOR in comparison with other Pt materials. The developed facile synthesis can be scaled up easily and should be highly valuable for routinely producing new metallic nanocages with large surface areas.

■ ASSOCIATED CONTENT

Ⓢ Supporting Information

Additional SEM, TEM, and HAADF-STEM images; N_2 adsorption/desorption isotherms; and wide-angle XRD data. This material is available free of charge via the Internet at http://pubs.acs.org.

■ AUTHOR INFORMATION

Corresponding Author

yamauchi.yusuke@nims.go.jp

Notes

The authors declare no competing financial interest.

■ ACKNOWLEDGMENTS

L.W. greatly appreciates NSF of China (No. 21273218).

■ REFERENCES

(1) (a) Hu, J.; Chen, M.; Fang, X. S.; Wu, L. M. *Chem. Soc. Rev.* **2011**, *40*, 5472–5491. (b) Zhang, F.; Shi, Y. F.; Sun, X. H.; Zhao, D. Y.; Stucky, G. D. *Chem. Mater.* **2009**, *21*, 5237–5243. (c) Liu, J.; Qiao, S. Z.; Hartono, S. B.; Lu, G. Q. *Angew. Chem., Int. Ed.* **2010**, *49*, 4981–4985. (d) Liu, J.; Hartono, S. B.; Jin, Y. G.; Li, Z.; Lu, G. Q.; Qiao, S. Z. *J. Mater. Chem.* **2010**, *20*, 4595–4601. (e) Sun, Z.; Kim, J. H.; Zhao, Y.; Bijarbooneh, F.; Malgras, V.; Lee, Y.; Kang, Y. M.; Dou, S. X. *J. Am. Chem. Soc.* **2011**, *133*, 19314–19317.

(2) (a) Bai, F.; Sun, Z. C.; Wu, H. M.; Haddad, R. E.; Xiao, X. Y.; Fan, H. Y. *Nano Lett.* **2011**, *11*, 3759–3762. (b) Peng, Z. M.; Wu, J. B.; Yang, H. *Chem. Mater.* **2010**, *22*, 1098–1106. (c) Song, Y. J.; Dorin, R. M.; Garcia, R. M.; Jiang, Y. B.; Wang, H. R.; Li, P.; Qiu, Y.; Swol, F.; Miller, J. E.; Shelnutt, J. A. *J. Am. Chem. Soc.* **2008**, *130*, 12602–12603. (d) Wang, H. R.; Song, Y. J.; Medforth, C. J.; Shelnutt, J. A. *J. Am. Chem. Soc.* **2006**, *128*, 9284–9285. (e) Fan, N. N.; Yang, Y.; Wang, W. F.; Zhang, L. J.; Chen, W.; Zou, C.; Huang, S. M. *ACS Nano* **2012**, *6*, 4072–4082. (f) Wang, J. X.; Ma, C.; Choi, Y. M.; Su, D.; Zhu, Y. M.; Liu, P.; Si, R.; Vukmirovic, M. B.; Zhang, Y.; Adzic, R. R. *J. Am. Chem. Soc.* **2011**, *133*, 13551–13557.

(3) (a) Liang, H. P.; Zhang, H. M.; Hu, J. S.; Guo, Y. G.; Wan, L. J; Bai, C. L. *Angew. Chem., Int. Ed.* **2004**, *43*, 1540–1543. (b) Peng, Z. M.; You, H. J.; Wu, J. B.; Yang, H. *Nano Lett.* **2010**, *10*, 1492–1496.

(4) (a) Lu, L. T.; Tung, L. D.; Long, J.; Fernig, D. G.; Thanh, N. T. K. *J. Mater. Chem.* **2009**, *19*, 6023–6028. (b) Sun, Q.; Ren, Z.; Wang, R. M.; Wang, N.; Cao, X. *J. Mater. Chem.* **2011**, *21*, 1925–1930. (c) Chen, H. M.; Liu, R. S.; Lo, M. Y.; Chang, S. C.; Tsai, L. D.; Peng, Y. M.; Lee, J. *J. Phys. Chem. C* **2008**, *112*, 7522–7526. (d) Huang, X. Q.; Zhang, H. H.; Guo, C. Y.; Zhou, Z. Y.; Zheng, N. F. *Angew. Chem., Int. Ed.* **2009**, *48*, 4808–4812. (e) Zhang, H.; Jin, M. S.; Liu, H. Y.; Wang, J. G.; Kim, M. J.; Yang, D. R.; Xie, Z. X.; Liu, J. Y.; Xia, Y. N. *ACS Nano* **2011**, *5*, 8212–8222. (f) Hong, J. W.; Kang, S. W.; Choi, B. S.; Kim, D.; Lee, S. B.; Han, S. W. *ACS Nano* **2012**, *6*, 2410–2419.

(5) (a) Wang, L.; Nemoto, Y.; Yamauchi, Y. *J. Am. Chem. Soc.* **2011**, *133*, 9674–9677. (b) Wang, L.; Yamauchi, Y. *J. Am. Chem. Soc.* **2009**, *131*, 9152–9153.

(6) (a) Lim, B.; Jiang, M. J.; Camargo, P. H. C.; Cho, E. C.; Tao, J.; Lu, X. M.; Zhu, Y. M.; Xia, Y. N. *Science* **2009**, *324*, 1302–1305. (b) Peng, Z. M.; Yang, H. *J. Am. Chem. Soc.* **2009**, *131*, 7542–7543.

(7) Habas, S. E.; Lee, H.; Radmilovic, V.; Somorjai, G. A.; Yang, P. D. *Nat. Mater.* **2007**, *6*, 692–697.

(8) (a) Kresge, C. T.; Leonowicz, M. E.; Roth, W. J.; Vartuli, J. C.; Beck, J. S. *Nature* **1992**, *359*, 710. (b) Yamauchi, Y. *J. Ceram. Soc. Jpn.* **2013**, *121*, 831–840.

(9) Song, Y. J.; Garcia, R. M.; Dorin, R. M.; Wang, H. R.; Qiu, Y.; Coker, E. N.; Steen, W. A.; Miller, J. E.; Shelnutt, J. A. *Nano Lett.* **2007**, *7*, 3650–3655.

(10) (a) Teng, X. W.; Liang, X. Y.; Maksimuk, S.; Yang, H. *Small* **2006**, *2*, 249–253. (b) Surendran, G.; Ramos, L.; Pansu, B.; Prouzet, E.; Beaunier, P.; Audonnet, F.; Remita, H. *Chem. Mater.* **2007**, *19*, 5045–5048.

(11) Yamauchi, M.; Kobayashi, H.; Kitagawa, H. *ChemPhysChem* **2009**, *10*, 2566–2576.

(12) (a) Liu, J.; Qiao, S. Z.; Chen, J. S.; Lou, X. W.; Xing, X. R.; Lu, G. Q. *Chem. Commun.* **2011**, *47*, 12578–12591. (b) Liu, J.; Qiao, S. Z.; Hu, Q. H.; Lu, G. Q. *Small* **2011**, *7*, 425–443. (c) Xia, Y. S.; Tang, Z. Y. *Adv. Funct. Mater.* **2012**, *22*, 2585–2593.

(13) (a) Wu, B. H.; Hu, D.; Kuang, Y. J.; Liu, B.; Zhang, X. H.; Chen, J. H. *Angew. Chem., Int. Ed.* **2009**, *48*, 4751–4754. (b) Sun, S. H.; Zhang, G. X.; Geng, D. S.; Chen, Y. G.; Banis, M. N.; Li, R. Y.; Cai, M.; Sun, X. L. *Chem.—Eur. J.* **2010**, *16*, 829–835.

(14) (a) Zhou, Z. Y.; Huang, Z. Z.; Chen, D. J.; Wang, Q.; Tian, N.; Sun, S. G. *Angew. Chem., Int. Ed.* **2010**, *49*, 411–414. (b) Tian, N.; Zhou, Z. Y.; Sun, S. G.; Ding, Y.; Wang, Z. L. *Science* **2007**, *316*, 732–735. (c) Lee, S. W.; Chen, S.; Sheng, W. C.; Yabuuchi, N.; Kim, Y.; Mitani, T.; Vescovo, E.; Shao-Horn, Y. *J. Am. Chem. Soc.* **2009**, *131*, 15669–15677.

(15) Liu, L.; Pippel, E.; Scholz, R.; Gosele, U. *Nano Lett.* **2009**, *9*, 4352–4358.